Solution Structure of Cardiotoxin V from *Naja naja atra*[†,‡,§]

Arun K. Singhal,[∥] Kun-Yi Chien,[⊥] Wen-guey Wu,[⊥] and Gordon S. Rule*[,∥]

Department of Biochemistry and Program in Biophysics, Box 440 Jordan Hall, University of Virginia, Charlottesville, Virginia 22908, and The Institute of Life Sciences, National Tsingh Hua University, Hsinchu, Taiwan 30043, Republic of China

Received March 15, 1993; Revised Manuscript Received May 20, 1993

ABSTRACT: Cardiotoxins are small proteins that are found in the venoms of snakes from the Elapidae family. These toxins are known to bind to and disrupt the organization, integrity, and function of the cell membrane. Most of the well-studied cardiotoxins cause depolarization of membrane potentials and/or lysis of red cells. In contrast, CTX V from *Naja naja atra* displays poor hemolytic activity but is proficient at inducing aggregation and fusion of sphingomyelin vesicles [Chien *et al.* (1991) *J. Biol. Chem. 266*, 3252–3259]. To determine whether the unique activity of this CTX is attributable to its tertiary structure, the solution structure of CTX V was determined by NMR methods. On the basis of these studies, this cardiotoxin has the same general topology as other members of the family, and thus its unusual properties do not arise from any gross structural differences that are detectable by solution NMR methods. Molecular dynamics calculations indicate that residues 36–50 show concerted fluctuations. On the basis of sequence similarity, we postulate that residues 30–34 are important in determining the specificity of cardiotoxins for fusion versus lysis of vesicles.

Cardiotoxins (CTX)[1] are a closely related family of peptide toxins found in the venom of snakes of the family Elapidae. The venom consists of multiple isoforms of cardiotoxins, neurotoxins, and phospholipases (A_2) (Bougis et al., 1986). Until recently, cardiotoxins were considered chaperone proteins for phospholipase A_2 because these proteins repeatedly copurified (Meldrum et al., 1965). However, this is no longer believed to be the case. Physiologically, cardiotoxins induce contraction and paralysis of frog heart, rat diaphragm, and rat atrial muscles. In vitro, these proteins are capable of inducing fusion and lysis of synthetic vesicles and disrupting cell membranes, causing either depolarization or lysis (Bougis et al., 1983; Meñez et al., 1990; Walker et al., 1990).

Cardiotoxins vary in length from 60 to 63 amino acids, and like the closely related family of venom neurotoxins, they are characterized by unusual compositional and structural properties for globular proteins. Proteins in this family generally contain a large number of Lys and Arg residues (12 in CTX V). The structure of CTX V_4^{II} from *Naja mossambica mossambica* has been determined by diffraction methods (Rees et al., 1990), and the solution structure of CTX XIIb from *N. mossambica mossambica* has been determined by NMR methods (Steinmeitz et al., 1988). The toplogy of these cardiotoxins is very similar and consists of three external loops which extend from a central core. The configuration of these loops is almost entirely antiparallel β-pleated sheet, while the core consists of four disulfide bonds and shows no defined secondary structure.

No definitive evidence exists which identifies the region of the protein involved in lipid binding, nor is it clear what molecular events occur after binding. Chemical modification studies (Ménez et al., 1990) have shown that, in CTX γ of *Naja nigricollis*, selective acylation of lysines implicates two regions of the protein as being important for binding to membranes. The first, contained within the first loop, is located in a highly variable region for this family of proteins. The second, contained within the second loop, is displaced significantly from residues 28–30, the second variable region in this family. Although the specific role of these regions in selectivity of action is not understood, direct interaction of residues in the first external loop with lipid is supported by fluorescence studies that show a blue shift of Trp11 and increased fluorescence emission intensity upon binding to membranes. These spectral changes are indicative of an increase in the hydrophobicity in the local environment (Vincent et al., 1978). The binding of CTX to membranes does appear to be at least partially electrostatic in nature. For example, CTX V_1^{II} from *N. mossambica mossambica* selectively interacts with negatively charged acidic phospholipids and does not bind at all to zwitterionic or positively charged lipids. However, CTX V binds preferentially to zwitterionic phospholipids with a strong dependence on salt concentration. This difference in selectivity has been postulated to be a consequence of a lysine to glutamic acid substitution at position 17 in the middle of an otherwise conserved six amino acid stretch in these proteins (Chien et al., 1991).

The actual mechanism of lysis, fusion, and/or depolarization is poorly understood, and it remains unclear whether surface binding is sufficient for activity. To understand further the mechanism of interaction between cardiotoxins and biological membranes, we have investigated the properties of a series of five cardiotoxins from the venom of *Naja naja atra* (Chien et al., 1991). The amino acid sequences of these toxins show a homology of 60% over the entire sequence, with regions of significantly lower similarity at positions 11–23 and 28–30. Although they show a large degree of overall sequence identity,

[†] This work was supported by a University of Virginia Biomedical Research Grant (RR-05431) to G.S.R. and by Grants NSC 78-0208-M007-10 and NSC 79-0208-M007-120 from the National Science Council (Taiwan) to W.-g.W. A.K.S. has been supported by a Medical Scientist Training Grant (2 T32GM07267-16).

[‡] The NMR-derived coordinates for two cardiotoxin V structures have been deposited in the Brookhaven Protein Data Bank; filenames: 1cvo and 1cvp.

[§] The authors can provide the unprocessed data in General Electric binary format. They are also willing to provide the distance constraint files and command files used in the DSPACE calculations. Please send electronic mail to gsr3g@virginia.edu.

* To whom correspondence should be addressed.

[∥] University of Virginia.

[⊥] National Tsingh Hua University.

[1] Abbreviations: CTX, cardiotoxin(s); NMR, nuclear magnetic resonance; NOE, nuclear Overhauser effect; RMS, root mean square.

0006-2960/93/0432-8036$04.00/0

these polypeptides possess distinctively different characteristics. One member of this series, CTX V, differs most significantly from the others at positions 25–30 and has a His residue inserted after residue 3. CTX V binds with greater affinity to zwitterionic sphingomyelins and induces aggregation and fusion of these vesicles. In contrast, CTX III from *N. naja atra* is inefficient at fusion of sphingomyelin vesicles but hemolyzes erythrocytes.

The ability of CTX V to cause fusion of sphingomyelin vesicles may be due to differences in either sequence or structure, or both. To investigate the possibility that the ability of CTX V to evoke fusion is related to a unique structural feature, we have determined the solution structure of CTX V using nuclear magnetic resonance methods. In addition, the molecular dynamics of CTX V have been characterized by measuring amide exchange kinetics and performing molecular dynamics calculations.

MATERIALS AND METHODS

Sample Preparation. Cardiotoxin V was purified from the venom of *N. naja atra* as previously described by Chien et al. (1991). Samples for NMR contained 4 mM protein, 10 mM phosphate, and 50 mM KCl. Data were obtained under the following conditions: pH 3.7, 45 °C; pH 4.2, 35 °C. The pH was measured in samples of 90% H_2O and 10% D_2O. For studies in the presence of 100% D_2O, the samples were freeze-dried, resuspended in 99.96% D_2O, and used without adjustment of pH.

Data Acquisition and Processing. All NMR measurements were performed on a General Electric Omega NMR spectrometer operating at a proton frequency of 500 MHz. The instrument was modified to provide high radio frequency power on the decoupler channel for spin-locking. Water suppression was normally accomplished by selective presaturation of the solvent line for 0.6 s. In this instrument the decoupler channel is coherent with the main radio frequency channel. Consequently, phase cycling of the decoupler by 180° after each scan improved the suppression of the water. Cross peaks from bleached α protons were obtained by use of the SCUBA prepulse sequence (Brown et al., 1988). Hypercomplex data (States et al., 1986) in the t_1 dimension was obtained by phase shifting the first pulse by 90°. 2K complex points were obtained in the t_2 dimension, and 256 complex points were obtained in the t_1 dimension. Data sets included COSY, NOESY, and TOCSY spectra in H_2O and NOESY, COSY, RELAY, and TOCSY spectra in D_2O. We also obtained a triple quantum filtered COSY in D_2O and a RELAY spectrum in H_2O and D_2O at pH 4.2 and 35 °C. TOCSY spectra were accumulated for all combinations of pH and temperature to assist in resolving spectral overlap. A total of 64 scans/t_1 slice were obtained for homonuclear correlation spectra (total experiment time 12 h), and 128 scans/t_1 slice were obtained for the NOESY spectra.

Proton–proton bond connectivities were detected using a number of standard two-dimensional single quantum correlation spectroscopic measurements. Single-bond connectivities were detected using double and triple quantum filtered COSY experiments (Müller et al., 1986). Two-bond connectivities were detected using a double quantum filtered RELAY experiment (Weber & Mueller, 1987). Multiple-bond connectivities were obtained using a TOCSY experiment (Braunschweiler & Ernst, 1983). The quality of the TOCSY spectra was improved by the use of z-filters (Rance, 1987). Two schemes were used for generating isotropic mixing. A WALTZ-16 (Shaka et al., 1983) scheme was used to generate coherence transfer over the complete range of chemical shifts, while a MLEV-17 (Bax & Davis, 1982) sequence with relaxation delays to remove NOE transfer effects (Griesinger et al., 1988) was used to produce cleaner spectra suitable for integration of cross-peak intensity for amide-exchange experiments. In both cases, a spin-lock field of 9 KHz was used. Spin-lock times of 25, 45, and 75 ms were used to generate spectra which displayed increasingly distant connectivities. Most amide–α connectivities were seen in the 25- and 45-ms spin-lock times, as were connectivities to the methyl protons of Ala. The longer spin-lock time of 75 ms was sufficient to produce a number of cross peaks between the amide and δ protons. Proton chemical shifts are referenced to HDO (35 °C, pH 3.7) at 4.8 ppm.

Proton–carbon correlated spectra were obtained using the heteronuclear multiple quantum sequence described by Bax et al. (1990). A dual channel reverse probe was used for this experiment. The proton pulse width was 20 μs, and the carbon pulse width was 24 μs. Decoupling of the carbons was accomplished with a garp 1–1 sequence with a decoupler field of 3000 Hz centered at the C_α region of the carbon spectrum. A total of 512 complex points were obtained. The spectrum was zero-filled once to give a resolution of 9.8 Hz per point in the ^{13}C dimension. A total of 64 scans were accumulated per t_1 slice. The resulting spectrum had a signal-to-noise ratio of approximately 5:1. Carbon chemical shifts are referenced to methanol at 49 ppm.

Through-space connectivities were detected using a NOESY pulse sequence (Jeener et al., 1979). Solvent suppression in NOESY spectra obtained in the presence of H_2O was accomplished essentially as described by Blake et al. (1991). The water resonance line was saturated for 0.6 s prior to the application of the SCUBA prepulse sequence. The mixing time in the NOESY sequence contained a 5-ms homospoil pulse at the beginning, a composite 180° pulse in the middle, and an additional 5-ms homospoil at the end of the mixing time. Mixing times of 50, 120, and 275 ms were used to obtain data to determine the time dependence of the NOE.

The samples used for amide-exchange studies were prepared by adjusting the pH of protein solutions in H_2O to pH 4.2 and then freeze-drying the protein. To initiate exchange, the dried protein was dissolved in a volume of D_2O equivalent to the amount of H_2O from which it was lyophilized. A TOCSY spectrum of 9-h duration was initiated immediately after the protein was dissolved. Additional spectra were accumulated at 24 and 48 h after the protein was dissolved. The exchange rates were obtained by integration of α-amide cross peaks in spectra gathered after commencement of exchange with D_2O. These intensities were normalized to the intensity of a cross peak between two nonexchangeable protons. The exchange was characterized as fast if the half-life of the amide proton was less than 3 h, intermediate if the half-life was between 3 and 30 h, and slow if the half-life was longer than 30 h.

NMR data processing was performed on a Sun Sparc Station using FELIX software (Hare Research, Bothell, WA). The final size of the two-dimensional homonuclear spectra was 2048 × 1024 points, giving a spectral resolution of 2.9 Hz/point in t_2 and 5.8 Hz/point in t_1. Streaks were removed from the spectral base-plane by subtracting the first and last 10 slices of the t_1 data from each of the t_1 time domain slices (Klevit, 1985).

Determination of Distance Constraints. Intraresidue distances between amide and α protons were determined on the basis of the scalar (J) coupling between these two protons. These couplings, which were estimated by analysis of the fine structure of the cross peaks in the TOCSY spectra, were used to fix ϕ angles for 27 of the amino acids as suggested by

Wüthrich et al. (1984). Briefly, ϕ angles were limited to -120 ± 40 or -65 ± 25 when the J coupling between the amide and α protons was ≥ 8 Hz or ≤ 5 Hz, respectively. All other distances were calculated on the basis of the time dependence of the buildup of NOE peak intensities. The rate of NOE increase as a function of mixing time was generated by integrating relevant 1D slices of the spectra and referencing the integrated intensities to a standard curve that was generated by averaging NOE peak intensities for geminal protons on Gly18, Gly39, Cys3, and Cys40. Interproton distances were calculated using the following equation:

$$d_{ij}^6 = \frac{I_{ij}}{I_{\text{ref}}} d_{\text{ref}}^6 \quad (1)$$

where I_{ij} and I_{ref} are the signal intensities of the NOE cross peak between protons i and j and the reference geminal protons, respectively, and d_{ij} and d_{ref} are the distances between protons i and j and the geminal protons, respectively. NOE cross peaks at long mixing times which did not show any intensity in the spectra obtained with a 50-ms mixing time were assumed to arise from spin-diffusion and were not used for distance constraints. The largest distance used in our constraint list was 4.5 Å, and 90% of the constraints were <3.5 Å. A range of ±6.5% of d_{ij} was used in defining the upper and lower bounds of the distance constraints. This range is larger than both the errors associated with the distance measurements themselves (estimated to be ±25% in the measurement of the NOE buildup rate) and the likely errors due to the use of the single-spin approximation for short interproton distances at these mixing times (Borgais et al., 1990).

Most of the interproton distances used were obtained from cross peaks between amide and α or β protons. Few constraints distal to the β protons are used primarily because the signal density is much greater in this region, making unambiguous assignment of cross peaks difficult. Also, as these cross peaks involve protons removed from the backbone, accurate determination of distances is more difficult because of wider variations in the rotational correlation times associated with the dipolar interaction.

Computation. Structural calculations were performed on a Silicon Graphics Personal Iris using DSPACE software (Hare Research). This software generates starting coordinates for structures based on a metric matrix distance geometry algorithm and then refines them by dynamical simulated annealing based on the penalty function discussed below. The distance geometry algorithm is based on the method of Crippen and Havel and is more fully described elsewhere (Crippen et al., 1983). The resulting structures were subjected to repeated cycles of simulated annealing (Clore & Gronenborn, 1989) based on the following target function:

$$P_{\text{total}} = P_{\text{exptl}} + P_{\text{covalent}} + P_{\text{nonbonded}} \quad (2)$$

where

$$P_{\text{exptl}} = \sum_{\text{NOEs}} K_{\text{NOE}} D^2 + \sum_{\text{Hbonds}} K_{\text{Hbond}} D^2 + \sum_{\text{torsion}} K_{\text{torsion}} D^2 \quad (3)$$

$$P_{\text{covalent}} = \sum_{\text{bonds}} K_{\text{bonds}} D^2 + \sum_{\text{angles}} K_{\text{angles}} D^2 + \sum_{\text{rigids}} K_{\text{rigids}} D^2 + \sum_{\text{chirals}} K_{\text{chirals}} D^2 + \sum_{\text{linears}} K_{\text{linears}} D^2 \quad (4)$$

and

$$P_{\text{nonbonded}} = \sum_{\text{vdw}} D^2 \quad (5)$$

and where D^2 is the square of the deviation of a value in the model from an ideal value and K is the weighting factor associated with that value. The abbreviations used in the above equations are NOE, NOE constraints; Hbond, noncovalent hydrogen bond constraints; torsion, torsional angle constraints; bonds, covalent bond lengths; angles, angles between bonds; rigids, geometry of aromatic rings; chirals, correct chirality of carbon atoms (where appropriate), linears, linearity of hydrogen bonds; and vdw, overlap in the van der Waals radii of nonbonded atoms. In case of bonds lengths, NOE constraints, hydrogen bonds, rigids, bond angles, and van der Waals potential, these deviations are defined as follows:

$$D^2 = (d - d_0)^2 \quad (6)$$

where d_0 is a single ideal value for bonds, angles, rigids, and van der Waals penalty functions and a range of allowable values for NOE and hydrogen bond penalty functions. In cases were the units of a variable are not Å (e.g., angles), the program converts the value of the variable to a distance. Therefore, the penalty values are given in units of Å^2. In addition to reporting penalties for terms in eq 3, DSPACE also calculates a penalty which arises from smoothing the data (smooth). A high penalty for this variable would indicate a large number of distances in the bounds matrix that are inconsistent with the triangle inequality.

The overall strategy for the generation of structures involved a number of steps. Interproton distances and hydrogen bonds contained in β-sheets were used to define the bounds matrix. The first generation of model structures were refined using only NOE constraints, covalent bonds, and van der Waal constraints (all weighted at 1) to minimize the total penalty of the structure. These structures were used to find errors in both assignments and distance measurements, which were detected by finding protons which showed repeated violations of greater than 0.2 Å in multiple models. These errors were corrected if warranted by the primary spectral data. In addition, these preliminary models were used to identify the location of additional hydrogen bonds. In the final structures additional penalty functions for ϕ angle restraints from J couplings, hydrogen bonds (where identified), and restraints to limit non-proline peptide bonds to a trans and planar ($180 \pm 5°$) configuration were included. No constraints were applied to peptide bonds preceding proline so that either a cis or a trans configuration would be allowable for these residues. Structures obtained from the final bounds matrix were subjected to five cycles (32 steps/cycle) of conjugate gradient minimization with all weighting factors set to 1. These structures were annealed in two steps. First, the weighting factors for bonds, angles, rigids, linears, Hbonds, and torsions were set to 40. The structures were then annealed (288 steps/cycle) at the following target penalties: 5000, 2500, 1000, and 500. The weighting factors were then lowered to 10 for bonds, 20 for angles, 1 for rigids, 1 for linears, 1 for Hbonds, and 20 for torsions. Annealing was continued at the following target penalties: 500, 250, and 100. The resultant annealed structures were then minimized. The higher weighting factors for torsions, bonds, and angles were used because it was noticed that within this refinement package lower weighting resulted in unacceptable deviations of torsional angles, bond lengths, and bond angles. The penalties reported in the final models were calculated using weighting factors of 1 for all variables.

Molecular modeling was performed using Sybyl molecular modeling software (version 6.0, Tripos Associates, St. Louis, MO) implemented on either a Silicon Graphics 4D/35 or a Silicon Graphics Personal Iris platform. All calculations are based on the Kollman United force field parameter set (Weiner et al., 1984, 1986). The empirical energy functions are as

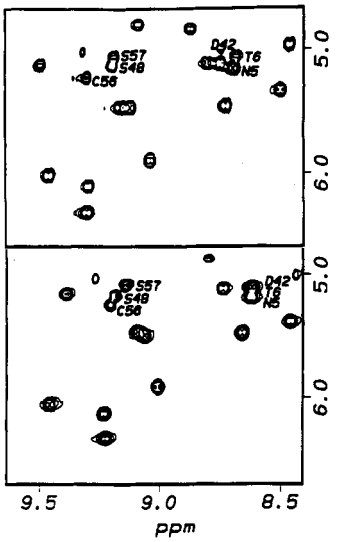

FIGURE 1: Effect of pH and temperature on the TOCSY spectra of cardiotoxin V. Shown are portions of the H_N–H region of TOCSY spectra of CTX-V. The top panel shows a spectrum taken at pH 4.2 35 °C. The bottom panel shows a spectrum taken at pH 3.7 and 45 °C.

described for the CHARMM program (Brooks et al., 1983). The coordinates of cardiotoxin V_4^{II} from *N. mossambica mossambica* were obtained from the Brookhaven National Laboratory Protein Data Bank. Chains A and B of the crystallographic dimer were treated separately and showed no differences in molecular dynamics calculations. The two NOE-derived structures with the lowest penalties were used as starting structures for cardiotoxin V. These structures were subjected to a maximum of 40 cycles of simplex minimization followed by 160 cycles of steepest descent minimization. Refinement was terminated when the root mean square gradient in energy between successive iterations of minimization was less than or equal to 2.5 kcal/(mol·Å^2). This structure was then equilibrated to the temperature of interest in a manner similar to that described by Brooks et al. (1983). Briefly, this involves 0.1 ps of molecular dynamics at 10 K intervals beginning at 5 K. During these cycles the starting velocities were randomly assigned on the basis of an appropriate Gaussian distribution for that temperature. Between cycles of molecular dynamics, the structure was minimized by steepest descent minimization for 100 cycles or until the RMS dropped to below 2.5 kcal/(mol·Å^2). When these models reached 315 K, a single cycle of 10.0-ps dynamics was performed with reassignment of random velocities every 0.5 ps and minimization of the structure every 2 ps by 200 cycles of steepest descent minimization with a 2.5 kcal/(mol·Å^2) termination option. The resultant structures were used in the calculation of molecular dynamics for 200 ps. Since the Shake option was enabled during this entire time to constrain covalent bonds to hydrogens, dynamic calculations were performed in 1-fs time steps (van Gunsteren & Berendsen, 1977).

RESULTS

Resonance Assignments. Sequential resonance assignments were obtained by following the general strategy described by Wuthrich (1986). The assignments of the geminal protons of Gly and Ser residues were confirmed with the proton–carbon correlated spectra. Spin systems with degenerate chemical shifts were resolved by changing the pH of the sample and the temperature during selected experiments. Examples of TOCSY spectra with three spin systems with a degenerate chemical shift, Asp42, Ser48, and Cys56, are shown in Figure 1. By varying the pH and temperature, these spin systems become nondegenerate and readily identifiable. The large pH-dependent chemical shift of the amide proton of Asp42 is equivalent to that seen in the NMR studies on CTXIIb by Steinmetz et al. (1988).

Sequence-specific assignments were initially identified on the 2D NOESY spectra with a 50-ms mixing time. The short mixing time allowed buildup of NOE signals in the closest through-space neighbors (<3.5 Å) with no detectable cross peaks that arise from spin diffusion. Residues with readily identifiable spin systems (e.g., Ala, Gly, Val, Ser, Thr) were used as starting locations for sequential assignments. As shown in Figure 2, 11 interruptions occur in this pattern (including the three C-terminal amino acids). Five of these interruptions are due to prolines, and of these, four were crossed solely by NOE cross peaks between the δ protons of proline and the α proton of the preceding residue. The two longest interruptions, Asn43–Pro45 and Lys60–Asn62, were assigned after the initial structure was built. The chemical shifts of most of the protons and of a number of the carbon atoms in cardiotoxin V are listed in Table I.

Structural Calculations. A total of 445 experimentally derived NOE distance constraints and 27 ϕ angle constraints were used to calculate the solution structure of CTX V. The locations of these constraints are schematically depicted in Figure 3. The existence of a number of hydrogen bonds, as indicated by protection from amide exchange, provided further constraints. One hundred structures were generated from these constraints by the metric matrix method. Of these models, 35% differed in the topology of the N-terminus; residues 12-15 were incorrectly placed adjacent to carboxyl-terminal residues, forcing the N-terminus to the exterior of the protein. These models failed to minimize to penalties of <100 Å^2. Although these models could be corrected by repeated cycles of randomization and simulated annealing, this process was computationally more expensive than generation of new starting structures. Therefore, these models were discarded. An additional 5% of the models showed flipped topology of the middle two strands of the second and the third loop, and the resulting structures were concave instead of convex (Figure 4B). These structures could not be corrected by randomization of the starting coordinates and were discarded because they also failed to minimize to penalties of <100 Å^2.

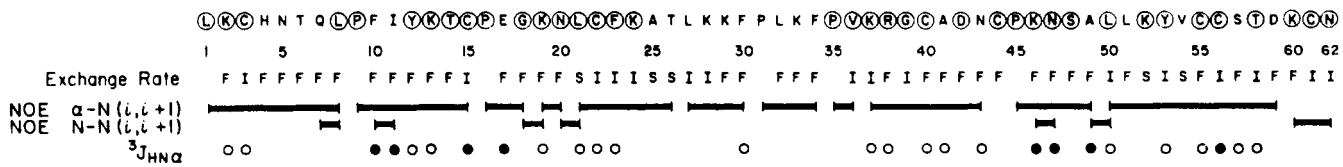

FIGURE 2: Summary of amide exchange rates, observed NOEs, and observed *J* coupling for cardiotoxin V. The primary sequence of CTX-V is shown in the top line. Circled residues are highly conserved in all 42 cardiotoxin sequences in the latest release of the Protein Identification Resource data base. The residue number is given in the second line. The amide exchange rate is given in the third line. Fast exchange is indicated by F; intermediate exchange, by I; and slow exchange, by S. These labels correspond to half-lives of less than 3 h, 3–30 h, and greater than 30 h, respectively. The observed NOEs between H_N and H_α protons and between H_N protons are indicated by the solid bars. The magnitude of the H_N–H_α scalar coupling is indicated by the bottom row of circles. Open circles represent scalar couplings which are greater than 8 Hz, and filled circles represent scalar couplings which are less than 5 Hz.

Table I: Proton and Carbon Chemical Shifts for Cardiotoxin V

residue no.	amino acid	amide	α	β	other[a]	carbon	residue no.	amino acid	amide	α	β	other[a]	carbon
1	Leu		4.29	1.69, 1.59	δCH$_3$ 0.90, 0.86		31	Pro		4.56	2.40	γCH$_2$ 2.10, 2.01	47.65 Cδ
2	Lys	8.66	5.48	1.39	γCH$_2$ 1.28	51.66 Cα						δCH$_2$ 3.63, 3.55	
					δCH$_2$ 1.51		32	Leu	8.41	4.60	1.87	γCH 1.74	
					εCH$_2$ 2.98							δCH$_2$ 1.08, 1.00	
3	Cys	8.74	5.13	3.05, 2.52		38.55 Cβ	33	Lys	7.89	4.33	1.99	γCH$_2$ 1.54, 1.50	
4	His	9.85	5.08	3.56, 2.82	2H 7.43							δCH$_2$ 1.60	
5	Asn	8.65	5.19	3.19, 2.33	γNH$_2$ 7.54, 6.73							εCH$_2$ 2.88	
6	Thr	8.62	5.11	4.58	γCH$_3$ 1.24		34	Phe	7.92	4.84	3.23, 3.12	2,4H 7.47	
7	Gln	8.89	4.30	2.51, 2.20	γCH$_2$ 2.10		35	Pro		4.57	2.19	γCH$_2$ 1.86, 1.70	
					δNH$_2$, 7.60, 6.99							δCH$_2$ 3.79, 3.08	
8	Leu	8.37	4.50	1.72, 1.69	γCH 1.44		36	Val	8.27	4.29	2.25	γCH$_3$ 1.15, 1.00	
					δCH$_3$ 1.07, 1.01		37	Lys	7.50	4.68	2.09, 1.98	γCH$_2$ 1.71	
9	Pro		4.21	1.99, 1.86	γCH$_3$ 1.30							δCH$_2$ 1.13, 1.06	
					δCH$_2$ 3.71, 3.61		38	Arg	8.79	4.44	1.55	γCH$_2$ 1.48	
10	Phe	7.57	4.94	3.44, 3.40	2,6H 7.41	50.33 Cα	39	Gly	6.39	4.18, 3.95			43.41 Cα
11	Ile	7.12	4.33	1.86	δCH$_2$ 1.15		40	Cys	8.97	5.96	3.58, 3.00		53.60 Cα
					δCH$_3$ 0.98		41	Ala	9.82	4.92	1.55		54.89 Cα
12	Tyr	8.48	5.41	2.70, 2.65	2,6H 6.95	53.39 Cα	42	Asp	8.67	5.14	3.04, 2.96		
					3,5H 6.80		43	Asn	8.124	4.79	2.65, 2.61	γNH$_2$ 7.52, 6.92	56.33 Cα
13	Lys	8.80	4.86	1.93, 1.79	γCH$_3$ 1.45, 1.35		44	Cys	9.18	4.73	3.11, 2.99		
14	Thr	8.95	4.73	4.21	γCH$_3$ 1.38		45	Pro		3.96	1.52, 1.27	γCH$_2$ –0.24, 0.65	48.15 Cδ
15	Cys	9.27	5.05	3.56, 3.00		49.23 Cα						δCH$_2$ 3.75, 2.81	
16	Pro		4.72	2.54, 2.32	γCH$_2$ 2.07	48.03 Cδ	46	Lys	7.80	4.23	1.93, 1.79	γCH$_2$ 1.74	
					δCH$_2$ 4.07, 3.59							δCH$_2$ 1.66	
17	Glu	8.62	4.17	2.14, 2.17	γCH$_2$ 2.58							εCH$_2$ 3.11	
18	Gly	8.99	4.44, 3.82			42.06 Cα	47	Asn	8.45	5.03	3.21, 3.04	γNH$_2$ 7.82, 7.42	50.36 Cα
19	Lys	7.79	4.48	3.07	γCH$_2$ 2.14, 1.54		48	Ser	9.20	5.18	4.63, 4.19		64.56 Cβ
					δCH$_2$ 1.24		49	Ala	8.85	4.32	1.61		
20	Asn	8.12	5.02	3.09, 2.84	γNH$_2$ 7.56, 7.02		50	Leu	7.98	4.67	1.81	γCH 1.69	
21	Leu	8.40	4.99	1.68	γCH 1.57	57.25 Cα						δCH$_3$ 1.10, 1.03	
					δCH$_2$ 0.94, 0.85		51	Leu	7.78	5.22	1.87	γCH 1.54	
22	Cys	9.24	6.14	3.28, 3.11		49.23 Cα						δCH$_3$ 0.91, 0.72	
23	Phe	9.22	6.34	3.36, 3.03	2,6H 7.00	52.97 Cα	52	Lys	8.96	4.74	1.84	γCH$_2$ 1.56, 1.30	
					3,5H 7.36		53	Tyr	9.08	5.52	3.12, 2.75	2,6H 6.92	55.25 Cα
24	Lys	9.39	5.17	2.09, 1.86	γCH$_2$ 1.69, 1.55							3,5H 6.37	
25	Ala	9.10	5.48	1.08		47.12 Cα	54	Val	8.86	4.70	2.11	γCH$_3$ 1.16	
26	Thr	9.04	4.83	4.35	γCH$_3$ 1.27		55	Cys	9.46	6.07	3.87, 3.23		52.80 Cα
27	Leu	8.68	4.72	1.99	γCH 1.82		56	Cys	9.22	5.25	3.75, 3.59		52.06 Cβ
					δCH$_2$ 1.14, 1.00		57	Ser	9.17	5.09	4.42, 3.99		62.23 Cβ
28	Lys	8.47	3.96	1.91, 1.74	γCH$_2$ 1.42, 1.63		58	Thr	7.65	4.84	4.41	γCH$_3$ 1.35	
					δCH$_2$ 1.69, 1.17		59	Asp	8.44	4.75	2.66, 2.32		
					εCH$_2$ 3.04		60	Lys	9.54	3.04	2.66, 2.32	γCH$_2$ 1.71, 1.41	
29	Lys	8.62	4.09	1.69	γCH$_2$ 1.55, 1.39							δCH$_2$ 0.83, 0.42	
					δCH$_2$ 1.18, 1.11							εCH$_3$ 1.98	
					εCH$_2$ 3.00		61	Cys	7.72	4.59	3.51, 3.80		47.58 Cβ
30	Phe	7.08	5.21	3.25, 2.97	2,6H 7.38		62	Asn	8.59	4.56	3.04, 2.51	γNH$_2$ 8.21, 7.97	

[a] Nomenclature of atoms is from Wüthrich (1986).

The penalties and deviations from ideal geometry of 20 models which refined to the lowest penalty are shown in Table II. The standard deviations in bond lengths, bond angles, and peptide bond torsional angles are 0.03 Å, 3.2°, and 6.8°, respectively. Of the 445 distance constraints used to build the models, approximately 150 were not violated in the models. Of the remaining distance constraints, approximately 80 distances violated lower bounds and approximately 200 violated upper bounds. The standard deviation of these distance violations was 0.21 Å for lower bounds and 0.26 Å for upper bounds, and in no case did a distance violation exceed 1 Å. The small deviations from ideal geometry and experimental distances indicate that the derived models are consistent with both ideal geometry and the experimental distances. Randomization of the coordinates by 10 Å, followed by annealing and minimization, did not result in any significant changes in the structures. This indicates that conformational space was adequately searched by initiating the simulated annealing with high penalties.

Five representative structures are shown in the stereodiagrams depicted in Figure 4. The protein consists of three external loops (residues 4–14, 23–39, and 45–54) which protrude from a central core containing eight cysteines involved in disulfide linkages: Cys3–Cys22, Cys15–Cys40, Cys44–Cys55, and Cys56–Cys61. Residues were considered to be a part of a β-strand if they possessed at least four of the following six characteristics: (1) strong α to amide proton NOE cross peaks on adjacent residues (<2.5 Å), (2) strong α to α proton NOEs across strands (≤2.7 Å), (3) medium amide proton to amide proton NOE cross peaks strands (<4.0 Å), (4) medium amide proton to α cross peaks across strands (<4.0 Å), (5) protected amide protons involved in hydrogen bonding across the sheet, or (6) *J* coupling between amide and α protons of greater than 8 Hz. On this basis, we have characterized residues 2–4 and 12–14 as forming one sheet and residues 21–28, 36–41, and 51–57 as forming a second sheet. Extensive protection of the amide protons from solvent exchange is noted in the β-pleated sheet involving the second and third external loops. However, the smaller sheet in the first loop shows minimal protection of the amide protons, suggesting that this sheet may be less stable than the second sheet. We find that residues 8–11, 17–20, 57–60 show patterns of NOEs characteristic of a type II turn. Similarly, residues 48–51 form a well-defined type I turn (Wüthrich, 1986). The carboxyl

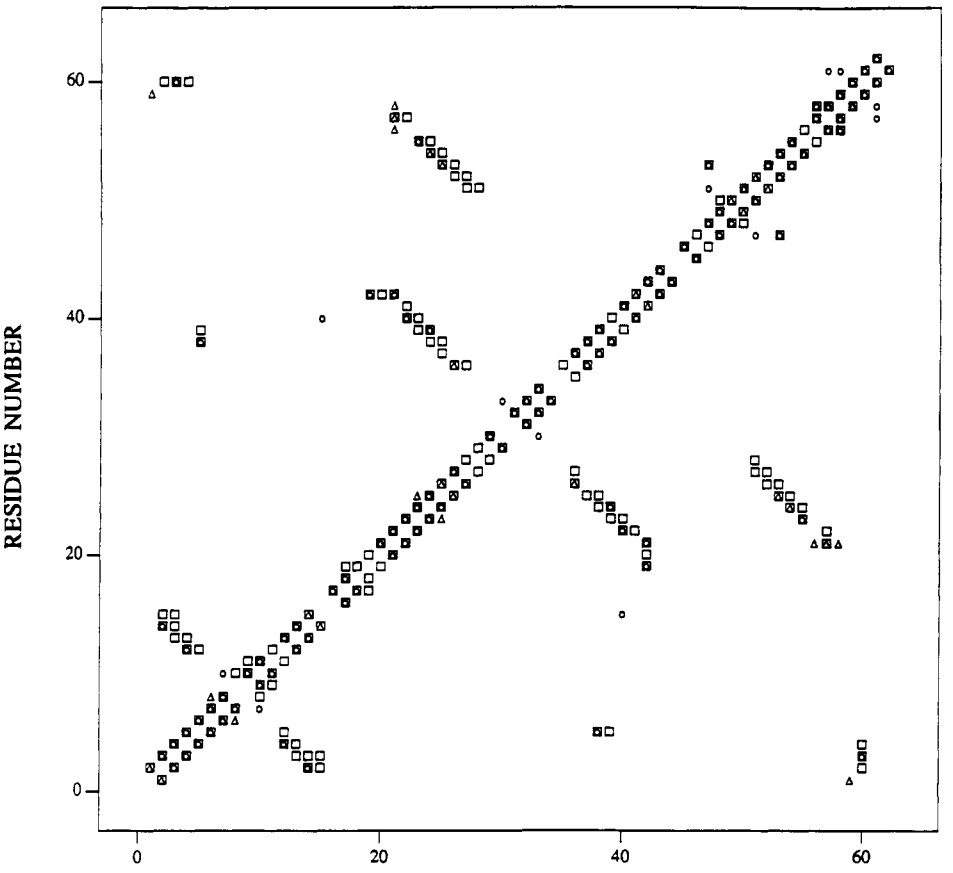

FIGURE 3: NOE distance constraints. The observed NOEs are indicated in this schematic diagram. The units of the axes are residues. Observed NOEs between main-chain protons (H_N and H_α) are indicated by squares. Observed NOEs between main-chain and H_β protons are indicated by circles. All other NOEs are indicated by open triangles.

Table II: Penalties and RMS Deviations[a]

violation	penalty ± SD (Å²)	mean violation ± SD
bond	0.6 ± 0.1	0.00 ± 0.03 (Å)
angle	0.4 ± 0.1	0.38° ± 3.20°
rigid	1.6 ± 0.3	
vdw	3.8 ± 0.8	
lowers	5.7 ± 0.5	0.21 ± 0.17 (Å)
uppers	21.2 ± 2.1	0.26 ± 0.20 (Å)
hbond	0.5 ± 0.1	
torsion	1.0 ± 0.3	0.86° ± 6.80°
smooth	1.5 ± 0.5	
chiral	0.0 ± 0.0	
linear	2.1 ± 0.4	
total	38.5 ± 2.4	

atoms superimposed[b]	RMS deviation (Å²)
β-sheet	0.9 ± 0.3
all backbone	1.4 ± 0.5
all atoms	2.4 ± 0.5

[a] Penalties and deviation from ideal geometry for the 20 models which refined to the lowest penalties. Violations are given for the deviation from ideal geometry for those bond lengths, bond angles, and torsional angles which would be affected by the NMR constraints. Violations for uppers and lowers arise from distances that exceeded the lower and upper distance bounds. [b] RMS deviations for positions of backbone atoms (C, CA, N) involved in β-sheet, all backbone atoms, and all atoms.

terminus is well defined by the disulfide linkage between Cys56 and Cys61 as well as multiple NOEs with the first and second external loops.

Amide Exchange Experiments. The measured exchange rates of the amide protons are given in Figure 5B. Of the 57 amide protons, only five showed half-lives of greater than 30 h. Sixteen showed intermediate exchange rates, and the remaining 36 amide protons exchanged rapidly. Of the protected amide protons, all five slowly exchanging protons and 12 of the protons with intermediate exchange rates are involved in β-pleated sheet formation. Thr58 also shows reduced amide exchange rates, although there is not an oxygen acceptor within 3 Å of the amide proton. Our models indicate that Thr58 is involved in hydrogen bonding with the sulfur Cys61.

Molecular Dynamics Calculations. The molecular dynamics calculations were carried out for 200 ps. Both CTX V from *N. naja atra* and CTX V_4^{II} from *N. mossambica mossambica* showed similar overall dynamics. Specifically, the second and third loops in both CTX V and CTX V_4^{II} undergo a concerted flip between two different conformations with the largest displacement localized to the external strands of the second and third loops. Representative members of both of these conformations of CTX V are shown in Figure 6. The distal tip of the third loop moves uniformly with the rest of the loop, preserving the turn. The distal tip of the second loop is equally mobile, but its motion is independent of the two conformations of the second and third loops. Residues 17–21 in CTX V are not mobile, possibly due to a salt bridge between Lys19 and Asp42. The corresponding lysine in CTX V_4^{II} retains the same topology but shows high mobility, possibly due to the replacement of aspartate by value, which removes a potential salt bridge.

DISCUSSION

In this paper we have determined the solution structure of CTX V from *N. naja atra.* The refined structure is characterized by a central core containing four disulfides.

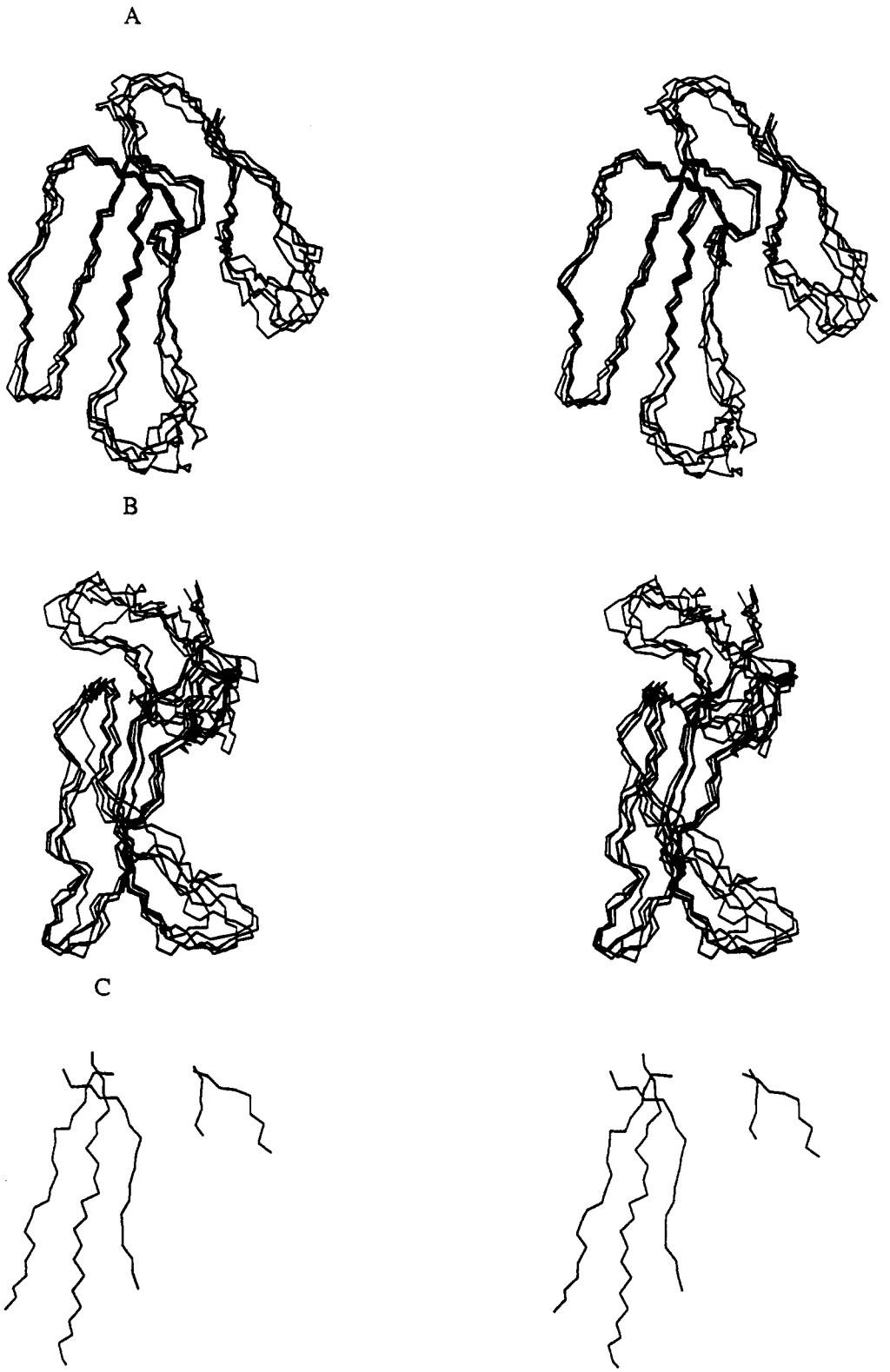

FIGURE 4: Solution structure of cardiotoxin V. Stereodiagrams of the tertiary structure of the backbone of cardiotoxin V, as determined by NMR distance constraints, are shown. (A) The external segments are from right to left. (B) The model is rotated 90° such that the third external segment is proximal and the first external segment is distal. The backbone atoms of residues 1–5, 13–15, 23–27, and 34–62 were overlayed to get the best RMS fit for these residues. The models and residues that were overlaid were chosen to maximize the spread in the structure of the distal tips of the external segments. (C) The orientation is similar to that in (A). Visible are the five strands involved in the two antiparallel β-pleated sheets. From right to left, residues 12–14 and 2–4 form the first sheet, and residues 36–41, 21–28, and 36–41 form the second sheet.

The overall structure is an oblate ellipsoid with three external loops (residues 4–14, 23–39, and 45–54) which radiate from the core. All three of these loops are involved in the formation of two antiparallel β-pleated sheets. The first sheet is within the first external loop and consists of residues 2–4 and 12–14. The second sheet is formed by the inner strands of the second and third external loops, residues 21–28 and 51–57, respectively, as well as the outer residues of the second external loop, residues 36–41. Also, four well-defined regular turns exist. Three of the turns are of type II and involve residues 8–11, 17–20, and 57–60, while residues 48–51 form a regular type I turn.

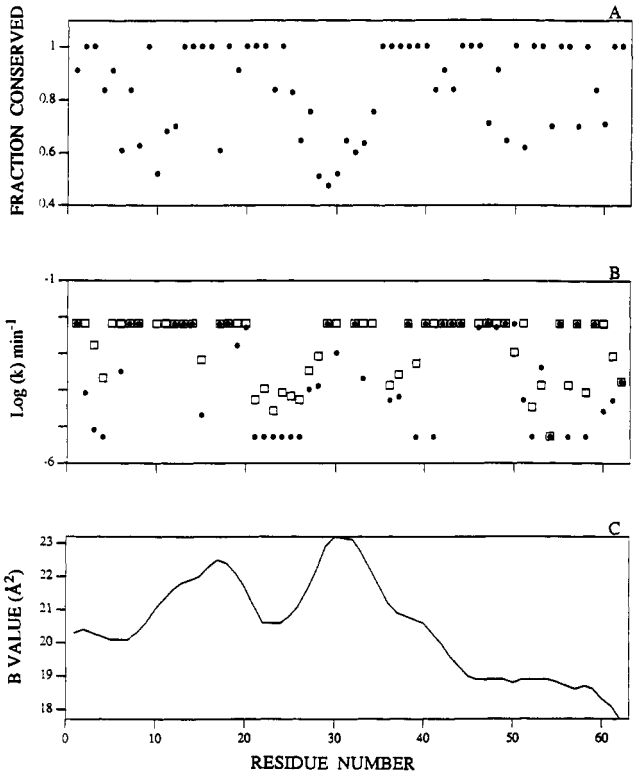

FIGURE 5: Properties of cardiotoxins. Panel A shows the conservation of residues among the 10 cardiotoxins found in the venom of *Naja naja atra* and *Naja mossambica mossambica* [see Chien et al. (1991) for sequences]. The fraction conserved was calculated by normalizing the second moment of the distribution of amino acid residues. If the same residue is found in all 10 cardiotoxins at a single position, then the fraction conserved is 1 for that position. If a different amino acid is found in all 10 cardiotoxins, then the fraction conserved is 0.32. Panel B shows the amide exchange rates for CTX V (open squares) and CTXIIb (solid circles). The amide exchange rates for CTXIIb were obtained from Otting et al. (1987). The exchange rates for CTX V have been reduced by a factor of 7 to account for the pH difference between the two sets of measurements. Panel C shows the crystallographic B factors for CTX_4^{II} obtained from Rees et al. (1990).

The solution structure of CTX V shows both similarities to and differences from the crystallographic structure of CTX V_4^{II} (Rees et al., 1990) and the ^{1}H NMR structure of CTXIIb (Steinmetz et al., 1988). The overall topology is the same in all three structures. The first β-pleated sheet in CTX V is shorter, however, than that found in the structures of the other cardiotoxins. This may be due to an insertion of His4 into the first external loop. The second β-sheet in CTX V is very similar to that seen in the X-ray structure of CTX V_4^{II}. In both proteins this sheet displays a strong right-handed twist with the concave surface bearing most of the hydrophobic residues, including Phe23 and Tyr53. The most significant difference between the structures of CTX V, CTXIIb, and CTX V_4^{II} is the relative position of residues 17–20 relative to 57–60. In the NMR structure of CTX V and the crystallographic structure of CTX V_4^{II} the distance between these residues is approximately 10 Å. In contrast, this distance in the NMR structure of CTXIIb is approximately 4–5 Å. Additionally, our NMR data show that the relative orientations of the three external loops are as well defined as the external loops in CTX V_4^{II} (see Figure 4). In contrast, the NMR structures of CTXIIb (Steinmetz et al., 1988) indicated that the relative orientations of these loops are less well defined in CTXIIb. To determine whether these structural differences between cardiotoxins are common will require the analysis of additional cardiotoxins by both NMR and crystallography.

On the basis of the solution structure of CTX V, it is apparent that the ability of various cardiotoxins to induce fusion of sphingomyelin vesicles is not related to any gross topological differences between these proteins. However, specific local structural differences exist between the different toxins, and these differences may be the cause of functional differences. The first external loop, containing residues 2–14, appears to be responsible for lytic activity. The hypothesis is supported by the observation that a peptide from the region of CTX IV from *N. mossambica mossambica* is sufficient for limited cytotoxicity, although its activity is approximately 30-fold less than that of the entire protein (Bougis et al., 1983). The corresponding region in CTX V does not have the extensive hydrogen-bonding network characteristic of this family because of an extra residue at position 4. The differences in the number of residues and hydrogen-bonding patterns may explain why CTX V is not efficient at lysis.

Residues in the second turn (17–19) may contribute to the specificity of lipid binding. Both CTX V_4^{II} from *N. mossambica mossambica* and CTX V contain a glutamic acid and a lysine in the second β-turn (positions 17 and 19, respectively, in CTX V) and bind zwitterionic phospholipids. These residues are postulated as being necessary for this type

FIGURE 6: Molecular dynamics calculations of cardiotoxin V. Molecular dynamics calculations were performed for 200 ps at 315 K. Shown are the backbone structures at 20-ps intervals. Two different conformations are apparent in the second and third external loops (indicated by arrows). These differences are most prominent in the external strands of these loops.

of specificity (Chien et al. 1991). The affinity of CTX for zwitterionic lipids is greater than that for negative phospholipids, whereas these affinities are reversed for CTX V_4^{II} (Bougis et al., 1983). Although the relative orientation of these two side chains is similar in both cardiotoxins, an additional ionic bond exists between Lys19 and Asp42 in CTX V, while an aspartate to valine substitution in CTX V_4^{II} prevents the formation of this ion pair. If Glu17 and Lys19 are important for determining specificity of lipid binding, the Lys19-Asp42 ion pair may be important in determining relative affinity for various charged lipids.

Lastly, the ability of cardiotoxins to fuse sphingomyelin vesicles may be related to specific residues at positions 30–34. Cardiotoxins that are similar in sequence to CTX V in this region are also efficient at fusing sphingomyelin vesicles (K.-Y. Chien and W.-g. Wu, manuscript in preparation). The sequence homology at positions 30–34 is generally low (Figure 5A), suggesting that differences in the primary sequence of this region may be related to differences in function. The amide exchange rates for both CTX V and CTXIIb are fast in this region (Figure 5B), and only a small number of NOE cross peaks for the residues are observed in the NOESY spectra. In addition, the average refined B values in the crystal structure of CTX V_4^{II} are highest for this region of the protein (Figure 5C). The NMR properties can be explained by either mobility or high solvent accessibility for this region. The crystallographic temperature factors can also be a result of mobility or static disorder. At this time we cannot distinguish between these two possibilities. However, the molecular dynamics calculations indicate that this region of the protein displays considerable mobility which appears to be independent of any conformational transitions involving the rest of the molecule. Although in previous work this region has been characterized as being unimportant in activity on the basis of chemical modification studies (Menez et al., 1990) and disorder in the crystal (Rees et al., 1990), we feel that this region may be more important in determining the specificity of action than previously believed because of the correlation between the primary sequence and the ability to cause fusion of lipid vesicles. Since this region of the protein appears to be unstructured both in solution and in the crystal lattice, it will be necessary to obtain information about the conformation of this region in a lipid environment to obtain a better understanding of the molecular basis of cardiotoxin-induced fusion of sphingomyelin vesicles.

ACKNOWLEDGMENT

We would like to thank Dr. J. Ellena for help in operating the spectrometer. We would also like to thank the Department of Chemistry (University of Virginia) for use of their 500-MHz spectrometer and The Molecular Simulations Laboratory for use of their computers for the molecular dynamics calculations.

REFERENCES

Bax, A., & Davis, D. G. (1985) *J. Magn. Reson. 65*, 355.
Bax, A., Ikura, M., Kay, L. E., Torchia, D. A., & Tschudin, R. (1990) *J. Magn. Reson. 86*, 304.
Blake, P. R., Park, J.-B., Bryant, F. O., Aono, S., Magnuson, J. K., Eccleston, E., Howard, J. B., Summers, M. F., & Adams, M. W. W. (1991) *Biochemistry 30*, 10885.
Borgais, A. B., Gochin, M., Kerwood, D. J., & James, T. L. (1990) *Prog. NMR Spectrosc. 22*, 83.
Bougis, P. E., Rochat, H., Pieroni, G., & Verger, R. (1981) *Biochemistry 20*, 7235.
Bougis, P. E., Tessier, M., Van Rietschoten, J., Rochat, H., Faucon, J. F., & Dufourcq, J. (1983) *Mol. Cell. Biol. 55*, 49.
Bougis, P. E., Manchot, P., & Rochat, H. (1986) *Biochemistry 25*, 7235.
Braunschweiler, L., & Ernst, R. R. (1983) *J. Magn. Reson. 53*, 521.
Brooks, B. R., Bruccoleri, R. E., Olafson, B. D., States, D. J., Swaminathan, S., & Karplus, M. (1983) *J. Comput. Chem. 4*, 187.
Brown, S. C., Weber, P. L., & Mueller, L. (1988) *J. Magn. Reson. 71*, 166.
Chien, K.-Y., Huang, W.-N., Jean, J.-H., & Wu, W.-G. (1991) *J. Biol. Chem. 266*, 3252.
Clore, G. M., & Gronenborn, A. M. (1989) *Crit. Rev. Biochem. Mol. Biol. 24*, 479.
Gregoret, L. M., Rader, S. D., Fletterick, R. J., & Cohen, F. E. (1991) *Proteins 9*, 99.
Griesinger, C., Otting, G., Wüthrich, K., & Ernst, R. R. (1988) *J. Am. Chem. Soc. 110*, 7870.
Havel, T., Kuntz, I. D., & Crippen G. M. (1983) *Bull. Math. Biol. 45*, 665.
Jenner, B. H., Meier, P., Bachmann, P., & Ernst, R. R. (1979) *J. Chem. Phys. 71*, 4546.
Klevit, R. E. (1985) *J. Magn. Reson. 62*, 551.
Meldrum, B. S. (1965) *Pharmacol. Rev. 17*, 393.
Ménez, A., Gatineau, E., Romestand, C., Harvey, A. L., Mouawad, L., Gilquin, B., & Toma, F. (1990) *Biochimie 72*, 575.
Müller, N., Ernst, R. R., & Wüthrich, K. (1986) *J. Am. Chem. Soc. 108*, 6482.
Otting, G., Steinmetz, W. E., Bougis, P., Rochat, H., & Wüthrich, K. (1987) *Eur. J. Biochem. 168*, 609.
Parker, J. M. R., Guo, D., & Hodges, R. S. (1986) *Biochemistry 25*, 5425.
Rance, M. (1987) *J. Magn. Reson. 74*, 557.
Rees, B., Bilwes, A., Samama, J. P., & Moras, D. (1990) *J. Mol. Biol. 214*, 281.
Shaka, A. J., Keeler, T., Frenkiel, T., & Freeman, R. J. (1983) *J. Magn. Reson. 52*, 335.
States, D. J., Haberkorn, R. H., & Ruben, D. J. (1982) *J. Magn. Reson. 48*, 286.
Steinmetz, W. E., Bougis, P. E., Rochat, H., Redwine, O. D., Braun, W., & Wüthrich, K. (1988) *Eur. J. Biochem. 172*, 101.
van Gunsteren, W. F., & Berendsen, H. J. C. (1977) *Mol. Phys. 34*, 1311.
Vincent, J. P., Balerna, M., & Lazdunski, M. (1978) *FEBS Lett. 85*, 103.
Walker, D. H., & Pike, L. J. (1990) *Biochim. Biophy. Acta 1055*, 295.
Weber, P., & Mueller, L. (1978) *J. Magn. Reson. 73*, 184.
Weiner, S. J., Kollman, P. A., Case, D. A., Singh, U. C., Ghio, C., Alagona, G., Profeta, S., & Weiner, P. K. (1984) *J. Am. Chem. Soc. 106*, 765.
Weiner, S. J., Kollman, P. A., Nguyen, D. T., & Case, D. A. (1986) *J. Comput. Chem. 7*, 230.
Wüthrich, K. (1986) *NMR of Proteins and Nucleic Acids*, John Wiley & Sons, New York.
Wüthrich, K., Billeter, M., & Braun, W. (1984) *J. Mol. Biol. 180*, 715.